stellarator news

Published by Fusion Energy Division, Oak Ridge National Laboratory
Building 9201-2 P.O. Box 2009 Oak Ridge, TN 37831-8071, USA

Editor: James A. Rome | Issue 45 | May 1996
E-Mail: jar@ornl.gov | Phone: (423) 574-1306 | Fax: (423) 574-0680

Trapped-Electron Transport Induced by ECRH in Stellarators

In most electron cyclotron resonant heating (ECRH) experiments in stellarators the resonant value of the magnetic field falls at a non-maximum field magnitude so that both transit and a fraction of trapped electrons gain energy from the wave. While the energy absorbed by transit electrons is assumed to be distributed evenly over the flux surface because of the fast parallel motion, the energy gained by helically (locally) trapped electrons remains confined (for a time determined by collisions) in the local well of the helical modulation of magnetic field and can be transported towards the plasma boundary owing to the radial drift.

The behavior of locally trapped electrons under the combined action of radio-frequency (RF) field and Coulomb collisions is described by the kinetic equation [1]

$$\frac{df}{dt} = \hat{L}_{QL} f + \hat{L}_C f \quad . \tag{1}$$

Here f is the bounce-averaged electron distribution function, $\hat{L}_{QL}$ is the quasilinear operator, and $\hat{L}_C$ is the bounce-averaged Coulomb collisional operator. We use variables

$$E = m_e c^2 \left[\left(1 + \frac{p^2}{m_e^2 c^2} \right)^{1/2} - 1 \right] - e\phi, \quad U = E - \mu B^* \ , \tag{2}$$

where ϕ is the scalar potential, $\mu = p_\perp^2 / 2 m_e E$, and B^* is the resonant value of magnetic field for electrons with $p = 0$. It was shown in ref [2] that in terms of E and U the quasilinear operator $\hat{L}_{QL}$ takes the one-dimensional form

$$\hat{L}_{QL} = \frac{1}{4\tau} \frac{\partial}{\partial E} |\Delta E|^2 \frac{\partial}{\partial E}, \tag{3}$$

where $\tau = \oint v_\parallel^{-1} dl$ is the bounce period of the trapped electron, l is a coordinate along the force line, and ΔE is the change in electron energy E on a single bounce oscillation, corresponding to a double transit through the resonance.

Because the pitch angle for locally trapped electrons is close to $\pi/2$, it is natural to keep only the angular term in the collisional operator $\hat{L}_C$ [3]. Averaging over the bounce period gives

$$\hat{L}_C = \frac{\nu_e T_e}{\nu x_e} \left[Z + \Phi\left(x_e^2 \right) \right] \frac{\partial}{\partial U} J \frac{\partial}{\partial U} \quad . \tag{4}$$

Here $\nu_e = 4\pi e^4 n_e \Lambda_e / m_e^2 v_T^3$, Λ_e is the Coulomb logarithm, the thermal electron velocity is determined as $v_{Te}^2 = 2T_e / m_e$, $x_e = v / v_{Te}$, Z is the ion charge number, $\Phi(x) = (1 - 1/2x) M(x) + M'(x)$, $M(x) = \frac{2}{\sqrt{\pi}} \int_0^x \sqrt{t}\ \exp(-t) dt$, and $J = m_e \oint v_\parallel dl$ is the longitudinal adiabatic invariant.

The expression for $|\Delta E|$ derived in ref [4], is

In this issue . . .

$$|\Delta E| = \frac{\ell^\ell}{\ell!}\pi e\, k_\perp^{\ell-1} L^\ell w_0^{1-3\ell/2} \left| K_+ Ai(-w) + iK_- Gi(-w) \right|^2, \qquad (5)$$

where ℓ is the ECRH harmonic number, and

$$\left\{ \begin{array}{c} Ai \\ Gi \end{array} \right\}(x) = \frac{1}{\pi} \int_0^\infty \left\{ \begin{array}{c} \cos \\ \sin \end{array} \right\}(t^3/3 + xt)\mathrm{d}t$$

are the Airy function and the Scorer function, respectively. In Eq. (5) we use the designations

$$L = B^* \left| \frac{\partial B}{\partial l} \right|^{-1}_{B=B^*}, \qquad (6)$$

$$w_0 = \left(\frac{2m_e}{E-U} \right)^{1/3} (\omega L)^{2/3}, \qquad (7)$$

$$w = \frac{w_0}{E-U}\left(U + e\phi - \frac{E^2}{2m_e c^2} \right) + \frac{k_\parallel^2 L^2}{w_0^2}, \qquad (8)$$

$$K_\pm = E_{\mathrm{eff}}^{(+)} \pm E \ . \qquad (9)$$

Here $E_{\mathrm{eff}}^{(\pm)}$ is the complex amplitude of the effective RF field $E_- + E_\parallel k_\perp v_\parallel / \omega$, referred to the point where resonance occurs for the given $(\pm)$ sign of $v_\parallel$; $E_\parallel$ is the parallel (with respect to the magnetic field) component of the RF electric field, and E_- is the circular component rotating in the same direction as the electrons. To find $E_\parallel$ and E_- it is necessary to take into account both the field inhomogeneity across the beam aperture and a spatial wave damping. For the fraction of electrons trapped deeply in the magnetic well, so that they never match the resonance condition (namely, for $w < 0$), we take

$$E_{eff}^{(+)} = E_{eff}^{(-)} = E_{eff}^{(\pm)}\big|_{w=0} \ .$$

The numerical solution of Eq. (1) was restricted to calculation of the stationary distribution function. When computing f, we use the parameters of the magnetic field, plasma and microwave beam typical for the ECRH experiments in the L-2 stellarator [5]. The numerical results show that, when the collisionless absorption due to transit electrons is high enough to provide strong ($\geq 95\%$) single-pass wave attenuation, only a small portion of the injected power reaches the region of exact electron cyclotron resonance. As a result, in this case, there is practically no energy exchange between trapped electrons and the wave. Otherwise, trapped electrons can absorb a noticeable amount of the injected power and transfer it towards the plasma periphery.

A typical profile of the radial energy flux $W(r)$ (normalized to the injected power P_0) associated with the superthermal tail of locally trapped electrons is shown in Fig. 1. The calculation is for the case of X-mode second harmonic heating ($\lambda = 0.4$ cm, magnetic field at the axis $B = 13$ kG) with quasi-transverse launch, taking the beam axis to cross the plasma column at 4.5 cm above the magnetic axis (which falls at the saddle point in the L-2 device). The beam intensity profile was taken in the form $I \propto \exp(-2\rho^2/\rho_0^2)$, with $\rho_0 = 2.75$ cm; the injected power was ~ 280 kW, and the electron density and temperature at the axis were $n_e = 1.5 \times 10^{13}$ cm^{-3} and $T_e = 0.7$ keV.

The decrease in W for $r > 8$ cm (beyond the beam aperture) appears as a result of the transfer of energy from trapped electrons to transit electrons owing to collisions. It is seen from Fig. 1 that, for the chosen beam and plasma parameters, a significant portion (about 10%) of the absorbed power can be transported towards the plasma periphery by trapped electrons. Note that when the heating region shifts towards the magnetic axis, this effect disappears because of a drastic decrease in the locally trapped electron population. The same effect occurs when the electron temperature is increased to 1 keV, because an increase in absorption due to transit electrons results in a strong attenuation of the high frequency field amplitude in the ECR region.

Therefore, our study demonstrates that energy transport by locally trapped electrons can provide a noticeable contribution to the energy balance in off-axis regimes of ECRH in stellarators.

REFERENCES

[1] A. S. Sakharov and M. A. Tereshchenko, Fiz. Plazmy **21** (1995) 99 [Plasma Phys. Reports, **21** (1995) 93].

[2] I. B. Bernstein and D. C. Baxter, Phys. Fluids **24** (1981) 108.

[3] L. M. Kovrizhnykh, Nucl. Fusion **24** (1984) 851.

[4] M. A. Tereshchenko, Kratkie Soobshcheniya po Fizike [Bull. Lebedev Phys. Institute], No. 11/12 (1994) 44.

[5] S. E. Grebenshchikov, Trudy IOFAN [Proc. General Phys. Institute], Moscow: Nauka **31** (1991) 37.

A. S. Sakharov and M. A. Tereshchenko
General Physics Institute
Russian Academy of Sciences
Vavilov Street 38, Moscow, 117942 Russia

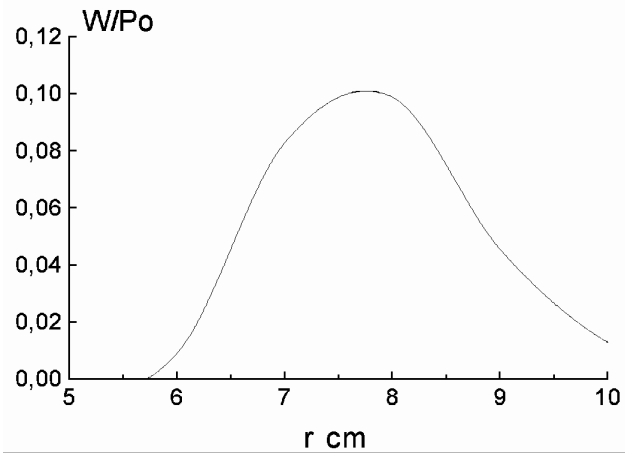

Fig. 1. Radial dependence of the energy flux of superthermal trapped electrons.

Comparison of parallel viscosity with neoclassical theory

In axisymmetric systems, the direction of the flow to be damped by the parallel viscosity is determined by the symmetry; that is, the flow in the direction without symmetry (poloidal flow) is damped. Thus, the viscosity coefficient appears in the expression for the parallel viscosity in order to determine the magnitude of the damping. On the other hand, in nonaxisymmetric systems, both the direction and the magnitude of the damping should be specified. Therefore the parallel viscosity (neglecting the heat flux) can be expressed as [1]

$$\langle \boldsymbol{B}\cdot\nabla\cdot\pi\rangle = \mu_a \langle \vec{U}_a\cdot\nabla\theta_a^*\rangle \quad , \tag{1}$$

where μ_a is the viscosity coefficient that mainly determines the magnitude of the damping and θ_a^* is an angle-like variable that mainly determines the direction of the damping:

$$\theta_a^* = \left(I+\langle G_{\rm BS}\rangle_a\right)\theta + \left(J-\tau\langle G_{\rm BS}\rangle_a\right)\phi \quad , \tag{2}$$

with $\theta(\phi)$ the poloidal (toroidal) angle in the Boozer coordinate system, $2\pi J$ ($2\pi I$ the poloidal (toroidal) current outside (inside) of the flux surface, τ the rotational transform,and $\langle G_{\rm BS}\rangle_a$ the geometric factor given in Ref. [2]. The subscripts a in θ_a^* and $\langle G_{\rm BS}\rangle_a$ indicates the particle species. The value of $\langle G_{\rm BS}\rangle_a$ depends on the collisionality of the species a.

In Compact Helical System (CHS) plasmas, there is no net toroidal current ($I = 0$). The first term of θ_a^* can be neglected in the plasma core ($\rho < 0.5$), because the toroidal velocity is dominant in these plasmas, with the tangential neutral beam injected in the toroidal direction. For instance, in a plasma with $R_{\rm ax}$ = 94.9 cm,$\langle G_{\rm BS}\rangle_i/(J/\tau)$ = 0.076 and 0.137, τ $(v_\phi/R)(v_\theta/r$ = 0.3 and 0.2 for ρ = 0.3 and 0.5, respectively. Thus, the parallel viscosity of the ions as given by Eq. (1) is simplified as

$$\langle B\cdot\nabla\cdot\pi_{\rm i}\rangle \simeq \mu_{\rm i} J\langle \vec{U}_{\rm i}\cdot\nabla\phi\rangle = \left(\frac{2n_{\rm i}m_{\rm i}\sqrt{2T_{\rm i}/m_{\rm i}}\ v_\phi J}{\lambda_{\rm PL}R}\right) \quad , \tag{3}$$

where $n_{\rm i}$, $m_{\rm i}$, and $T_{\rm i}$ are the ion density, mass, and temperature, respectively. In CHS, ions are in the plateau collisionality regime and the viscosity coefficient $\mu_{\rm i}$ is given by $2n_{\rm i}m_{\rm i}(2eT_{\rm i}/m_{\rm i})^{1/2}/\lambda_{\rm PL}$ and $\lambda_{\rm PL}$ is defined in Ref. [2] as

$$\frac{1}{\lambda_{\rm PL}} = \left[\frac{\sqrt{\pi}\ (J+\tau I)}{2\langle B^2\rangle}\right]\times \tag{4}$$

$$\left\langle \langle \hat{\boldsymbol{n}}\cdot\nabla\boldsymbol{B}\rangle \sum_{mn}\frac{1}{|m\tau+n|}\left(\frac{1}{B}\hat{\boldsymbol{n}}\cdot\nabla\boldsymbol{B}\right)_{mn}\exp^{i(m\theta+n\phi)}\right\rangle$$

where $\hat{\boldsymbol{n}}$ is normalized vector in the direction of magnetic field and m and n are the poloidal and toroidal period numbers. Here we define a parallel viscosity coefficient for the toroidal flow, $\mu_\parallel$, as

$$\mu_\parallel \equiv \frac{\langle \boldsymbol{B}\cdot\nabla\cdot\pi_{\rm i}\rangle}{Bm_in_iv_\phi} = \frac{2\sqrt{2eT_i/m_i}\ J}{\lambda_{\rm PL}RB} \quad . \tag{5}$$

These values are closely related to the three-dimensional magnetic field structure. In the large aspect-ratio limit, it is simplified to $\mu_\parallel = \pi^{1/2}\gamma^2(R/n)(2eT_i/m_i)^{1/2}$ with the modulation of the magnetic field strength γ and the toroidal period number, n. The modulation of the magnetic field strength, γ, is defined as $\gamma^2 = \langle(\partial B/\partial s)^2\rangle/B$, where s is the length along the magnetic field line and the angle brackets $\langle\ \rangle$ indicate a flux surface average operator.

Figure 1 shows neoclassical parallel viscosity coefficient profiles calculated from magnetic structure including finite-beta effects in the plateau regime in CHS. The parallel viscosity coefficient increases very rapidly towards the plasma edge, which yields strong damping of the toroidal rotation velocity, regardless of the position of the vacuum magnetic axis, $R_{\rm ax}$. As the magnetic axis is shifted outward, the parallel viscosity coefficient increases even near the plasma center. The increase in the parallel viscosity coefficient obtained by shifting the plasma from 89.9 cm, where there is negligible ripple, to $R_{\rm ax}$ = 97.4 cm, where the helical ripple is more than 2%, is one order of magnitude near the plasma center.

The parameter dependence of the viscosity coefficient is studied by changing the field ripple to determine whether

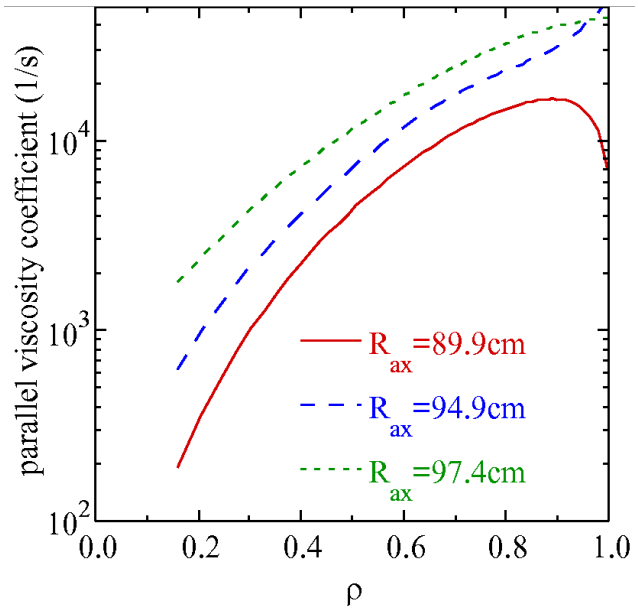

Fig. 1. Radial profile of the parallel viscosity coefficient in CHS when the vacuum magnetic axis is $R_{\rm ax}$ = 89.9, 94.9, and 97.4 cm.

it is neoclassical. The damping of toroidal rotation velocity due to charge-exchange loss can be neglected except at the plasma periphery. Here we introduce the effective viscosity coefficient μ_{eff} (s^{-1}) as an indication of the strength of the damping of the central velocity by the parallel and perpendicular viscosities, $n_i m_i \mu_{\parallel} v_{\phi}$, and $-n_i m_i \mu_{\perp} \nabla^2 v_{\phi}$, in the plasma, where $\mu_{\parallel}$ (s^{-1}) and $\mu_{\perp}$ (m^2/s) are the parallel and perpendicular viscosity coefficients, respectively. The effective viscosity coefficient μ_{eff} is defined as $\mu_{eff}^{-1} = v_{\phi}(0) m_i n_e(0) / f_{NBI}($(, where $f_{NBI}(0)R$ is the torque due to neutral beam injection. If there is no perpendicular viscosity, $\mu_{eff} = \mu_{\parallel}$. Figure 2 shows the inverse of μ_{eff} as a function of magnetic field ripple, revealing the γ^2 dependence predicted by neoclassical theory in the region where the neoclassical parallel viscosity becomes dominant, $\gamma > 0.2$. For $\gamma < 0.2$, the neoclassical parallel viscosity becomes small and the anomalous perpendicular viscosity becomes dominant. The anomalous perpendicular viscosity coefficient, $\mu_{\perp}$, to fit the measured data is 2 m^2/s.

Since the plasma is in the plateau regime, the neoclassical parallel viscosity coefficient should be independent of collisionality (electron density or ion temperature) except for v_{th} in Eq. (3). In order to check, the effective viscosity coefficient was measured at various densities. In this density scan, the ion temperature was more or less constant. As seen in Fig. 3, the effective viscosity coefficient shows at most only a weak dependence on the electron density when the modulation of B is large ($\gamma = 0.42$ m^{-1}) and the neoclassical parallel viscosity is dominant. However, when the modulation of B is small ($\gamma = 0.12$ m^{-1}) and the neoclassical parallel viscosity is negligible, the effective viscosity coefficient has a strong dependence on electron density. This density dependence is a feature of anomalous transport, because a strong density dependence is also observed in the energy transport, which is governed by anomalous transport.

The parallel viscosity coefficient derived from the toroidal rotation velocity shows good agreement with the neoclassical parallel viscosity coefficient calculated with three-dimensional magnetic structure, when the perpendicular viscosity with a coefficient $\mu_{\perp}$ of 2 m^2/s is added to the neoclassical viscosities.

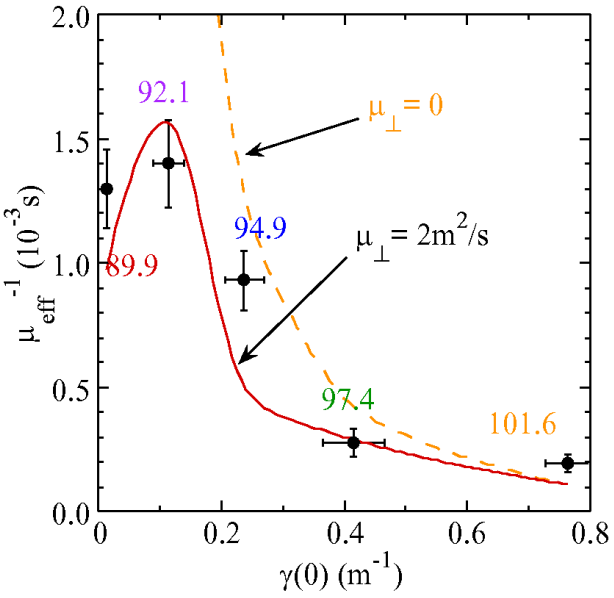

Fig. 2. Inverse of the effective viscosity coefficient as a function of the magnetic field modulation strength, γ, with the prediction of the neoclassical parallel viscosity, $n_i m_i \mu_{\parallel} v_{\phi}$, and neoclassical parallel viscosity plus anomalous perpendicular viscosity, $n_i m_i \mu_{\parallel} v_{\phi}$ - $n_i m_i \mu_{\perp} \nabla^2 v_{\phi}$ ($\mu_{\perp}$ = 2 m^2/s), in CHS.

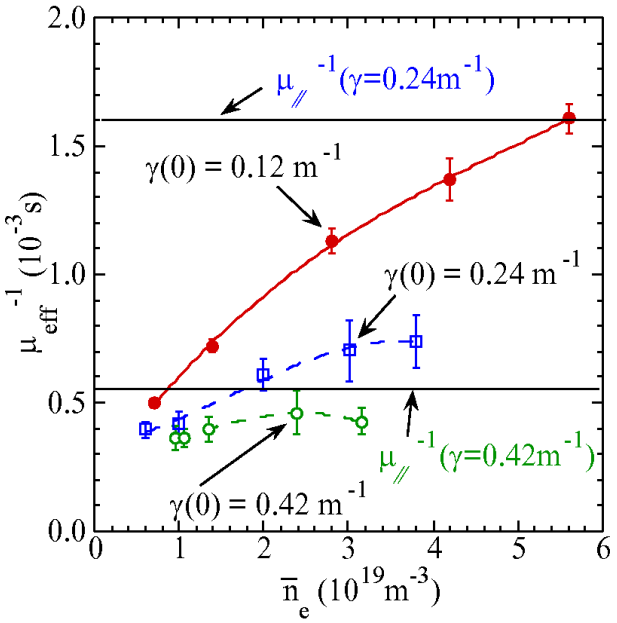

Fig. 3. Inverse of the effective viscosity coefficient as a function of the line-averaged density.

References

[1] N. Nakajima, M. Okamoto, and M. Fujiwara, Kakuyugo-kenkyu **68** (1992) 503.

[2] K. Y. Watanabe, N. Nakajima, M. Okamoto, K. Yamazaki, Y. Nakamura, and M. Wakatani, Nucl. Fusion **35** (1995) 335.

K. Ida, N. Nakajima
National Institute for Fusion Science
Nagoya 464-01 Japan

Simulation of the W7-X edge plasma using the B2-code

The island divertor concept [1] uses sufficiently large islands at rational ι values, e.g., $\iota = 5/5$ in Wendelstein VII-X (W7-X), and their accompanying separatrix at the boundary to divert the outstreaming plasma and guide it towards the target plates. The magnetic configuration of W7-X can be used to create an inherent divertor without the need for an additional coil system. Compared with the tokamak divertor, the topology of each island sector corresponds to a single-null configuration. Differences from the tokamak exist mainly in geometry values owing to the larger aspect ratio and the multiple X-points: In W-7X, the connection length is longer, the distance between target and separatrix is smaller, and the ratio of the volumes around the X-points and in the private flux region to the total scrape-off layer (SOL) volume is larger. Three-dimensional (3-D) effects are introduced by the toroidal variation of the island shape and by the segmented target plates. The latter causes parallel gradients and local effects of neutral particles.

One approach to modeling the SOL is via the multifluid code B2 [2]. The code is based on a rectangular grid that is generated approximately for W7-X as shown in Fig. 1. Because of the five-fold symmetry it is sufficient to do the calculations in one island region equal to a sector of 1/5 of the poloidal circumference.

Because B2 is a 2-D code, the geometry of the plasma edge must be averaged (distances) or integrated (areas and volume) in the toroidal direction. Figure 2 shows the averaged island geometry used in our calculations. The target plates intersect the islands and the private flux region. The bottom boundary of the grid is connected with the core plasma. The left and right sides are connected with the neighboring islands and are simulated in the calculations by symmetry planes.

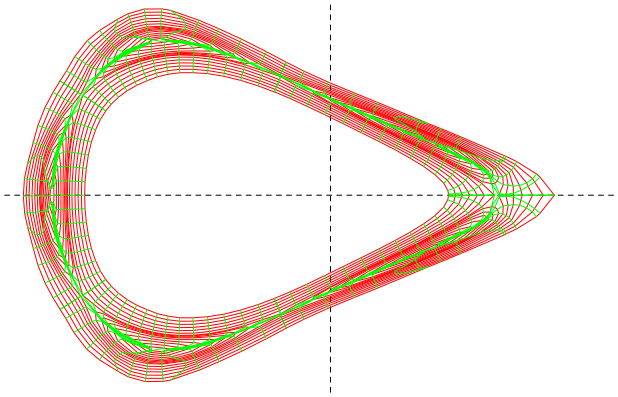

Fig. 1. Grid of the W7-X edge structure at a toroidal angle of $\phi = 36°$. Because of $\iota = 5/5$, each of the five islands closes upon itself after one toroidal transit. The islands have an identical 3-D shape with a toroidal phase shift of one field period.

The system is symmetric about the vertical midplane of the figure; this symmetry is not employed in the modeling in order to see the influence of statistics in our calculations. The following boundary conditions are used: the plasma density and the power flux (2 MW per island, fixed in all cases) are prescribed at the border to the main plasma in the radial direction; zero gradients of all plasma variables are assumed at the symmetry planes in the poloidal direction; low temperature (2 eV) and zero density are preset at the boundary towards the wall (private region and O-points); the condition $V_{\|} = c_s$ is used for the parallel velocity at the targets. The cross-field thermal diffusivity for electrons and ions is set to 1 m^2/s, and the particle diffusivity is set to 0.5 m^2/s. The present study is made with a simple neutral particle recycling

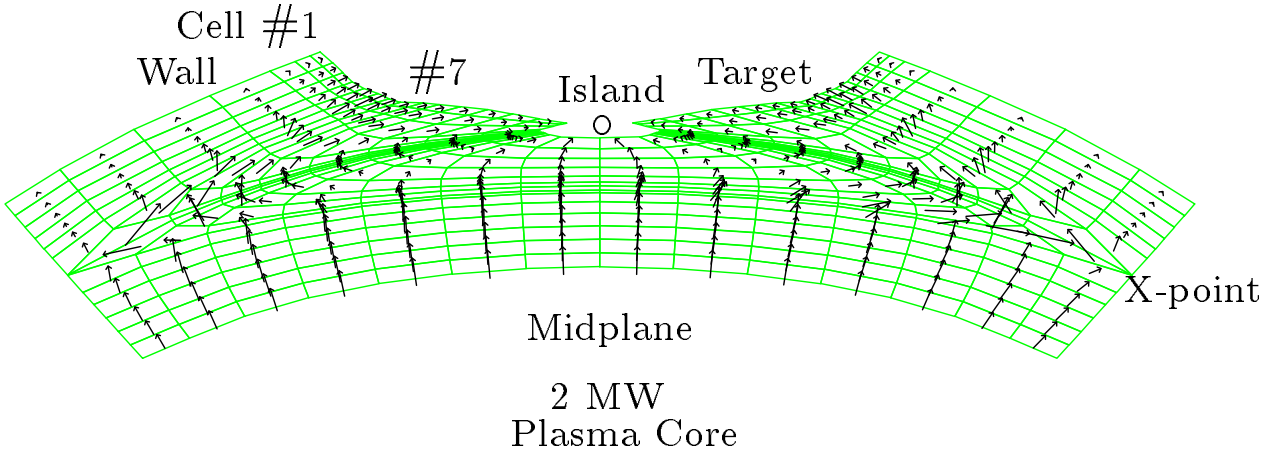

Fig. 2. Geometry of one island sector averaged in the toroidal direction. The left and right sides of the sector are connected with the neighboring islands. The arrows show the calculated power flow.

model using recycling coefficients of 1 at the wall and 0.98 at the targets.

In the first part of this investigation, no impurity radiation is assumed. The plasma density at the separatrix midplane is varied from 1.5 to $5 \times 10^{19} m^{-3}$. Figure 3 gives the calculated temperature and density at the target plate vs the radial cell number. In the case with the low separatrix midplane density, rather high temperatures and a low density at the target result. With increasing midplane density, a steep decrease of the temperature at the targets and a drastic increase of the density follow. At a midplane density of 2.5×10^{19} m^{-3} (middle curves of Fig. 3) the density at the target is about 5 times higher than at the separatrix and is increasing still further towards the O-point of the island, thus showing that the high-recycling regime is already attainable at a moderate density. In Fig. 4 the power density is shown for the three separatrix density values. Because of the 2-D nature of the calculation, the results are averaged values along the wetted length of the target plates. For comparison, the maximum value derived by the 3-D Monte Carlo model with constant parameters everywhere is about 8 MW/m^2 [1] with a toroidal average of about half of the maximum value.

In the second part of this study, impurity transport and radiation losses of carbon with a prescribed concentration of 1.7% at the separatrix midplane and a recycling factor of 1 everywhere are taken into account. The electron density is set to 3.1×10^{19} m^{-3} at the separatrix midplane. The power radiated by carbon is 350 kW; it is concentrated in front of the target plates. This power loss significantly reduces the electron temperature in the private flux region while the ion temperature stays nearly constant there, see Fig. 5. In the island region (right side of the figure) both temperatures are reduced. The maximum power density at the targets is reduced by about 25% compared to the results without impurity radiation, and the plasma density is enhanced there, see Fig. 6. However, owing to the thermal forces there is no density increase of carbon from the midplane to the targets as is seen for deuterium. We expect to enter the detachment regime with higher edge radiation power.

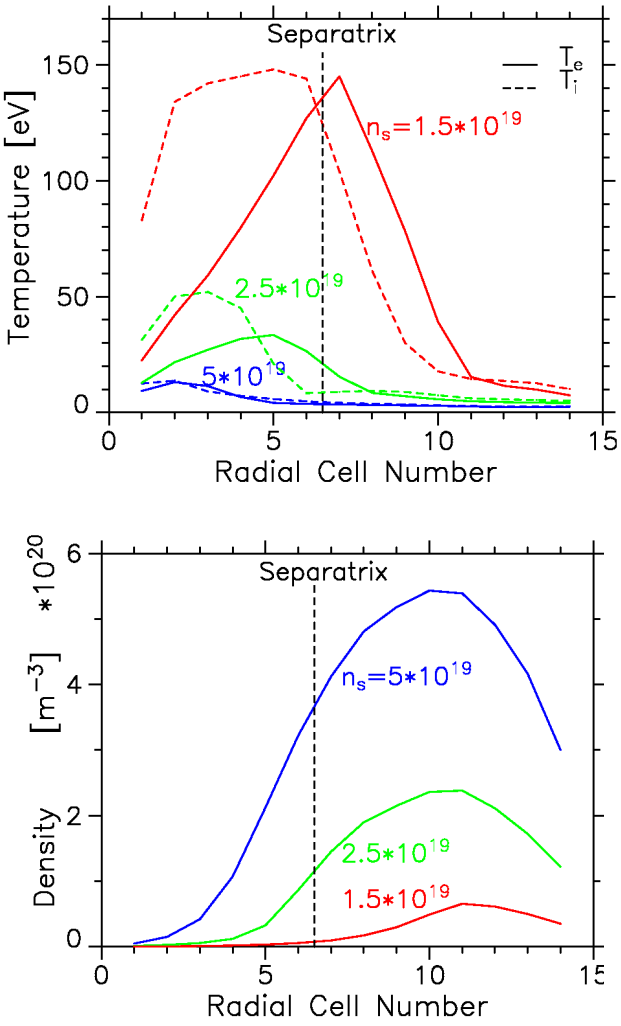

Fig. 3. Effect of the separatrix density n_s at the midplane on the temperature (top) and density (bottomt) at the target plate vs the radial cell number. Cells 1 to 6 are in the private flux region, cells 7 to 14 are inside the island. For the middle curve, the maximum density inside the island increases by a factor of 9 compared with $n_s = 2.5 \times 10^{19}$ m^{-3}.

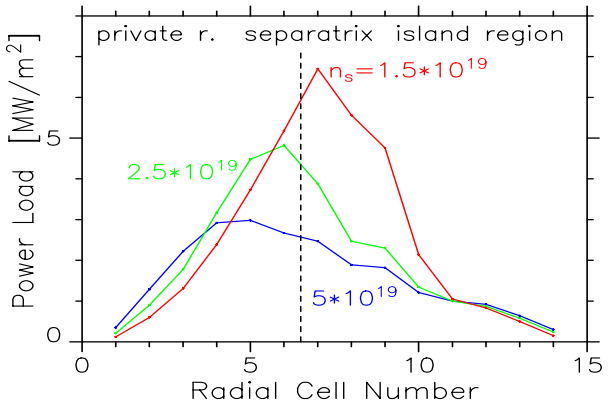

Fig. 4. Power load on the target plates for three different separatrix densities. Impurity radiation is not included in these calculations.

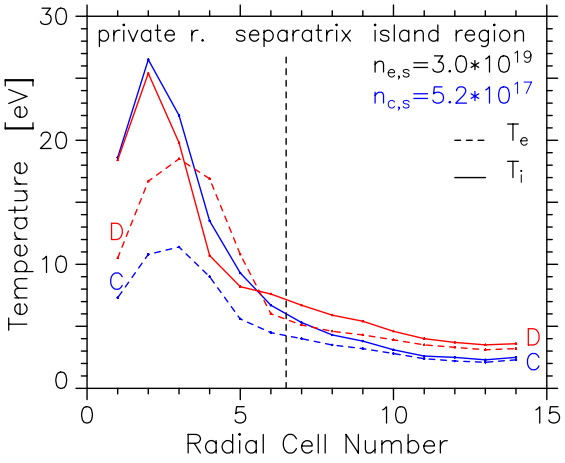

Fig. 5. Temperature at the target plate for a pure deuterium plasma (D) and a deuterium plasma with carbon as impurity (C). Midplane separatrix densities are 3×10^{19} m^{-3} and 5.2×10^{17} m^{-3}, respectively.

In summary:

- The B2 code has been employed for the first time to model a stellarator field.
- The high-recycling regime is attainable at densities above 2–3 $\times$ 10^{19} m^{-3} without radiation.
- The calculated heat loads on the targets are comparable with values calculated with a 3-D Monte Carlo code.
- Radiation of carbon is localized in front of the target plates. It reduces the temperature and power load and increases the density in this region.
- The calculated carbon density does not show an increase from the midplane to the targets as seen for deuterium.

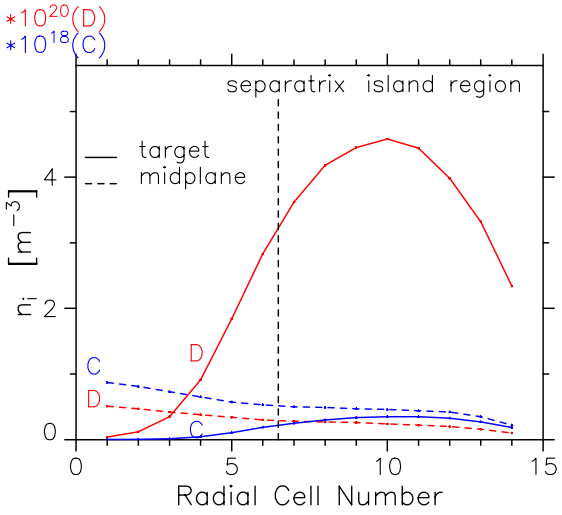

Fig. 6. Density at the midplane (dashed lines) and at the target for deuterium (D) and for carbon (C). Note the different scales for the two species, with separatrix values of 3×10^{19} m^{-3} for D and 5.2×10^{17} m^{-3} for C.

References

[1] J. Kisslinger, et al., In Proc. 21st EPS, Montpellier, 1994, **18B**, I, 368.

[2] B. J. Braams, Ph.D. Thesis, Rijksuniversiteit Utrecht (1986).

J. Kisslinger for the W7-X Team
Max Planck Institut für Plasmaphysik
EURATOM Association
Garching bei Müunchen, Germany

E-mail: jok@ipp-garching.mpg.de
Phone: 0049-89-3299-1232